

GRB 090426: the environment of a rest-frame 0.35-s gamma-ray burst at a redshift of 2.609

Emily M. Levesque,^{1,2*} Joshua S. Bloom,³ Nathaniel R. Butler,^{3†} Daniel A. Perley,³
S. Bradley Cenko,³ J. Xavier Prochaska,⁴ Lisa J. Kewley,¹ Andrew Bunker,⁵
Hsiao-Wen Chen,⁶ Ryan Chornock,³ Alexei V. Filippenko,³ Karl Glazebrook,⁷
Sebastian Lopez,⁸ Joseph Masiero,¹ Maryam Modjaz,^{3‡} Adam Morgan³
and Dovi Poznanski³

¹*Institute for Astronomy, University of Hawaii, 2680 Woodlawn Dr., Honolulu, HI 96822, USA*

²*Smithsonian Astrophysical Observatory, 60 Garden St., Cambridge, MA 02139, USA*

³*Department of Astronomy, 601 Campbell Hall, University of California, Berkeley, CA 94720-3411, USA*

⁴*Department of Astronomy and Astrophysics, UCO/Lick Observatory, University of California, 1156 High Street, Santa Cruz, CA 95064, USA*

⁵*Department of Astrophysics, Oxford University, Keble Road, Oxford OX1 3RH*

⁶*Department of Astronomy & Astrophysics, University of Chicago, Chicago, IL 60637, USA*

⁷*Centre for Astrophysics and Supercomputing, Swinburne University of Technology, PO Box 218, Hawthorn, VIC 3122, Australia*

⁸*Departamento de Astronomía, Universidad de Chile, Casilla 36-D, Santiago, Chile*

Accepted 2009 September 18. Received 2009 September 15; in original form 2009 July 8

ABSTRACT

We present the discovery of an absorption-line redshift of $z = 2.609$ for GRB 090426, establishing the first firm lower limit to a redshift for a gamma-ray burst (GRB) with an observed duration of < 2 s. With a rest-frame burst duration of $T_{90z} = 0.35$ s and a detailed examination of the peak energy of the event, we suggest that this is likely (at > 90 per cent confidence) a member of the short/hard phenomenological class of GRBs. From analysis of the optical-afterglow spectrum we find that the burst originated along a very low H I column density sightline, with $N_{\text{H I}} < 3.2 \times 10^{19} \text{ cm}^{-2}$. Our GRB 090426 afterglow spectrum also appears to have weaker low-ionization absorption (Si II, C II) than ~ 95 per cent of previous afterglow spectra. Finally, we also report the discovery of a blue, very luminous, star-forming putative host galaxy ($\sim 2L_*$) at a small angular offset from the location of the optical afterglow. We consider the implications of this unique GRB in the context of burst duration classification and our understanding of GRB progenitor scenarios.

Key words: galaxies: ISM – gamma-rays: bursts.

1 INTRODUCTION

The early emergence of a two-class bifurcation in the high-energy properties of gamma-ray bursts (GRBs; Kouveliotou et al. 1993) gave rise to the supposition that two distinct ‘progenitors’ could be responsible for the lion’s share of such events (e.g. Zhang & Mészáros 2004). While observations directly link long-duration soft-spectra GRBs (LSBs) to the death of young massive stars (Hjorth et al. 2003; Stanek et al. 2003; see Woosley & Bloom 2006 for a review), less-strong circumstantial evidence (based on physical associations with more evolved galaxies) suggests that at least some fraction of short-duration hard-spectra GRBs (SHBs) are

due to older progenitors (Berger et al. 2005; Fox et al. 2005; Hjorth et al. 2005; Bloom et al. 2006; Bloom & Prochaska 2006; Prochaska et al. 2006).¹ Whether SHBs are due to the coalescence of two neutron stars, other compact degenerate binaries, some combination of these models or something else entirely is an open question (cf. Lee & Ramirez-Ruiz 2007).

Several lines of evidence now suggest that the true progenitor diversity does not map with one-to-one correspondence to the

¹ In this paper, we will use the term ‘SHB’ to denote this phenomenological class of GRBs as first identified in the Burst and Transient Source Experiment (BATSE) sample. This is distinct from a simple cut on duration or hardness, since the populations are known to overlap to varying degrees with different instruments. Furthermore, identification with a class does not necessarily imply identification with a particular progenitor, even though most LSBs have been associated with massive stars and a few SHBs have been associated with old populations.

*E-mail: emsque@ifa.hawaii.edu

†GLAST/Einstein Fellow

‡Miller Fellow.

two-class phenomenological landscape.² In particular, there appear to be many more than just two progenitors. For example, a small fraction of SHBs probably originate from massive flaring activity of extragalactic magnetars (highly magnetized neutron stars; Abbott et al. 2008; Hurley 2008; Chapman, Priddey & Tanvir 2009). Either similar magnetar activity (or perhaps a flaring accretion-powered system) from objects in our own Galaxy may occasionally create LSBs as well (Castro-Tirado et al. 2008; Kasliwal et al. 2008). Classification of individual events even among the two well-established cosmological groups has proven extremely difficult, not only in the overlap region of the duration–hardness diagram where the population distributions merge [at around 1–2 s for *Swift*/Burst Alert Telescope (BAT)] but even for much longer duration events. Indeed, some of the same SHBs which have been used to link this phenomenological class to older, evolved galaxies actually have observed total durations (as measured by T_{90} , the interval over which 90 per cent of the burst counts are observed) of over 100 s due to a component of extended emission (EE) that follows the initial spike. At least two LSBs at low redshift, GRB 060505 and GRB 060614, were not accompanied by observable supernovae despite intense follow-up campaigns (Fynbo et al. 2006; Gehrels et al. 2006), and it is still debated whether these events group most naturally with short-duration events, long-duration events or a new class entirely (e.g. Jakobsson & Fynbo 2007; Levesque & Kewley 2007; Lu, Huang & Zhang 2008; Thöne et al. 2008; Xu et al. 2009 and others). Most recently, the two highest redshift GRBs detected to date, at $z = 6.7$ and 8.2 (Greiner et al. 2009; Salvaterra et al. 2009; Tanvir et al. 2009; Zhang et al. 2009), were observed to have rest-frame durations of <2 s, yet few have argued that these events did not arise from massive stars.

To date, the strongest evidence that many SHBs and LSBs arise from a different progenitor population comes from analysis of their respective host galaxy associations. The host galaxies of long-duration GRBs have, universally, been observed to have blue colours, subsolar interstellar medium (ISM) metallicities, and strong emission features associated with high specific star formation rates (Stanek et al. 2006; Modjaz et al. 2008; Berger 2009; Savaglio, Glazebrook & LeBorgne 2009). The burst position, when well constrained, is nearly always at small offset (Bloom, Kulkarni & Djorgovski 2002) and typically traces the brightest regions of the host galaxy (Fruchter et al. 2006), which itself is typically blue and morphologically disturbed (Wainwright, Berger & Penprase 2007). Fruchter et al. (2006) also find that LGRB host galaxies have lower luminosities on average compared to the galaxy population probed by surveys at similar redshifts. In contrast, the host galaxies of short-duration GRBs to date have been observed to be much more heterogeneous, including both star-forming and non-star-forming hosts. Afterglow offsets range from negligible to many times the half-light radius of the putative host (Prochaska et al. 2006; Berger 2007; Bloom et al. 2007; Troja et al. 2008).

It is against this backdrop that GRB 090426 enters the scene. With an observed duration of $T_{90} = 1.28 \pm 0.09$ s (Section 2), based on its observer-frame duration alone it groups more closely with the SHB class, an identification that is further bolstered when its high redshift of $z = 2.609$ (Section 4) is considered, implying a rest-frame duration of only 0.35 s that is unambiguously within the range of classical SHBs. By contrast, the most convincing host associations for SHBs are at $z < 1$ (although see Berger et al. 2007

and a discussion of the potentially high-redshift SHB GRB 060121; de Ugarte Postigo et al. 2006; Levan et al. 2006).

Irrespective of the phenomenological classification or the physical origin of this event, we report on an optical spectrum of the afterglow – the first ever reported for an event with an observed duration of <2 s – which shows evidence of an environment quite unlike that of most (but not unprecedented among) GRBs of long duration with spectroscopic observations. We also present the results from our campaign of late-time imaging and spectroscopy, which identify the highly ultraviolet (UV)-luminous host galaxy of this event. All of the values and conclusions in this paper are consistent with our GCN Circulars³ but should be considered to supersede our previous work on this event.

2 THE DISCOVERY AND CLASSIFICATION OF GRB 090426

At 12:48:47 on 2009 April 26,⁴ the BAT (Barthelmy et al. 2005) onboard the NASA *Swift* satellite (Gehrels et al. 2004) was triggered on GRB 090426. The X-Ray Telescope (XRT; Burrows et al. 2005) began observing the field at 84.6 s after the trigger, and the Ultraviolet/Optical Telescope (UVOT; Roming et al. 2005) followed at 89 s after the trigger. UVOT detected a candidate optical afterglow at $\alpha = 12^{\text{h}}36^{\text{m}}18^{\text{s}}.07$, $\delta = +32^{\circ}59'09''.6$ (J2000), which was reported by Cummings et al. (2009) 13.8 min after the burst trigger. The optical counterpart at these coordinates was also confirmed 43.5 min after the burst by Xin et al. (2009) based on observations obtained 76 s after the burst with the Tsinghua–National Astronomical Observatories Telescope at Xinglong Observatory in China. The Sloan Digital Sky Survey (SDSS) shows no object near the position of the afterglow; the closest object is a faint and extended source at $\alpha = 12^{\text{h}}36^{\text{m}}19^{\text{s}}.49$, $\delta = +32^{\circ}59'05''.5$ (J2000), 18 arcsec away from the optical afterglow with a photometric redshift of $z \sim 0.3$ (D’Avanzo et al. 2009). As detailed in Section 4.1, we obtained a spectrum of the afterglow 1.1 h after trigger, independently discovering the optical afterglow by inspection of the guider and acquisition frames and determining an absorption redshift of $z = 2.609$ (Levesque et al. 2009). Later, Thöne et al. (2009) confirmed this afterglow detection and redshift with a Very Large Telescope (VLT) spectrum observed 12.3 h after the trigger.

2.1 The short-duration/hard-spectrum bifurcation in *Swift*

The question of which phenomenological classification to ascribe to GRB 090426 is obviously an important one. To do so, we examine the hardness–duration distribution of *Swift* and BATSE (from which the original classification scheme was derived). Here, we measure hardness by fitting a Band et al. (1993) model to the BAT spectrum and extracting the best-fitting νF_{ν} peak energy E_{peak} (see Butler et al. 2007). Fig. 1 (top panel) displays the durations and hardnesses for 398 *Swift* GRBs detected by *Swift* between 2004 December and 2009 April.

It has been noted previously (e.g. Curtis et al. 2006; Zhang & Choi 2008) that there is only weak evidence for a distinct short-duration class in the *Swift* sample considered alone. Band (2006) suggests that the discrepancy arises primarily as a result of the *Swift* increased sensitivity (relative to BATSE) to long GRBs, which tends

² See Bloom, Butler & Perley (2008) and Zhang et al. (2007) for a discussion of GRB classification, both physical and phenomenological.

³ The GCN system <http://gcn.gsfc.nasa.gov/> is managed and operated by Scott Barthelmy.

⁴ UT dates are used throughout this paper.

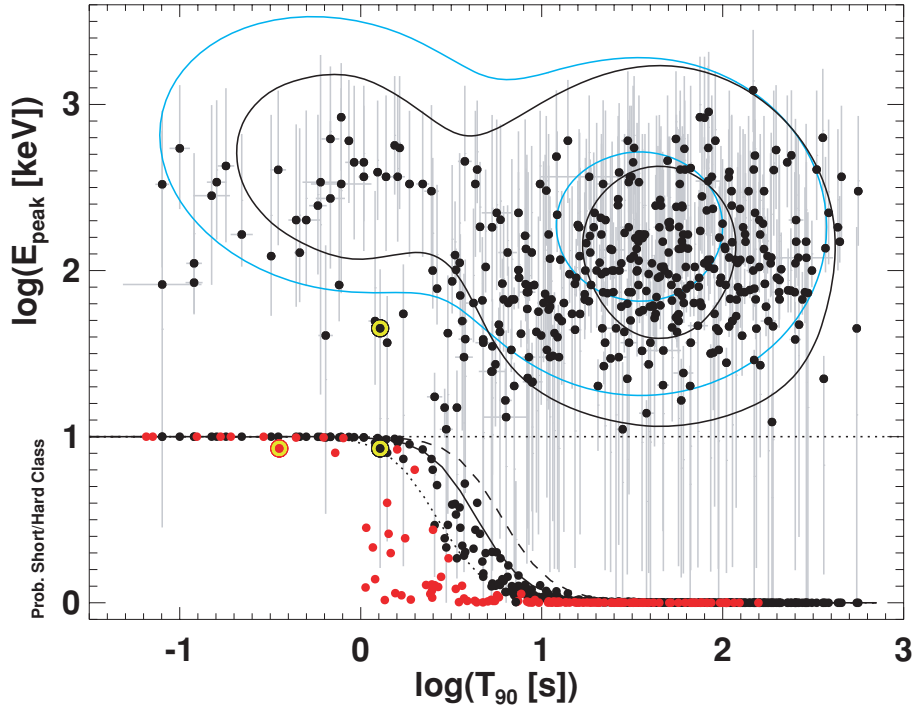


Figure 1. Top: the T_{90} durations and E_{peak} values for 398 *Swift* GRBs. Overplotted is a double-Gaussian model fit to data from BATSE (blue; 50 per cent peak probability and 5 per cent peak probability contours). The black curves show the relative distortion expected for these distributions appearing in *Swift*, given the relative satellite detection efficiencies (see Band 2006). There are relatively \sim three times fewer short/hard GRBs expected in the *Swift* sample. GRB 090426 is highlighted and circled in yellow. Bottom: the ratio of Gaussians defines the probability that a given burst will belong to the short/hard class. Red circles give the host-frame $T_{90z} = T_{90}/(1+z)$ values for 138 GRBs with measured spectroscopic redshifts. The solid black curve shows the projection on to the abscissa of the solid distribution in the top panel. Dashed and dotted curves are also shown to display the E_{peak} dependence of the curve at two E_{peak} values ($E_{\text{peak}} = 1$ MeV and $E_{\text{peak}} = 20$ keV, respectively). GRB 090426 T_{90} and T_{90z} are circled in yellow.

to make detected short-duration GRBs a factor of ~ 3 less common in *Swift* relative to BATSE. We explore this possibility in detail here by correcting the observed *Swift* number distributions for sensitivity. The cyan curves in the top panel of Fig. 1 show a double Gaussian fit – one Gaussian to represent the short/hard class and one Gaussian to represent the long/soft class – to the distributions from BATSE, while the solid black curves show how these curves transform once we apply a relative rate correction using the sensitivity curves from Band (2006). The bottom panel of Fig. 1 shows the projection of these curves on to the T_{90} duration axis, which provides a probabilistic classification between the two populations. Additional discussion of these calculations can be found in Appendix A and in Butler et al. (in preparation).

2.2 Classification by T_{90} and E_{peak} for GRB 090426

We download the raw, unfiltered *Swift* BAT data for GRB 090426 from the *Swift* Archive.⁵ Our reduction of these data to science-quality light curves and spectra using standard *Swift* tools are detailed by Butler et al. (2007). We employ calibration files from the 2008 October 26 BAT release. The BAT signal in the 15–350 keV band consists of a single, narrow emission spike of duration $T_{90} = 1.28 \pm 0.09$ s ($T_{50} = 0.48 \pm 0.06$ s). The spectrum in the 15–150 keV band is well modelled ($\chi^2/\nu = 54.18/45$) as a single power law with photon index $\beta = -2.02^{+0.25}_{-0.28}$ and an energy fluence (15–350 keV) of $2.5^{+0.4}_{-0.3} \times 10^{-7}$ erg cm⁻². Using our Bayesian

methodology (Butler et al. 2007) to extrapolate to an approximately bolometric energy release in the 1–10⁴ keV band (source frame), we find $E_{\text{iso}} = 4.2^{+5.9}_{-0.4} \times 10^{51}$ erg, with a νF_{ν} spectral peak energy of $E_{\text{peak}} = 45^{+57}_{-43}$ keV (observer frame).

Above, we map a two-class model (Gaussian G_1 for the short/hard class and Gaussian G_2 for the long/soft class) justified based on comparing BATSE data to the *Swift* sample. We will now apply this classification to *Swift* GRBs and to GRB 090426 in particular. Importantly, the precise factor dictating the relative *Swift*/BATSE number distribution at a given value of E_{peak} and T_{90} – which we derive approximately above as arising solely from variations in the satellite sensitivities – does not enter into this calculation. We only need to know the ratio of the probabilities, which means the factor drops out of the relative classification calculation. In principle, the relative rate factor could also depend on variations with redshift of the intrinsic source populations (ignored above) at fixed values E_{peak} and T_{90} , but we make the simplifying assumption here that this can be ignored.

It is important to demonstrate that our derived E_{peak} and T_{90} values from *Swift* are sufficiently similar to those derived from BATSE. Because we have defined E_{peak} in a similar fashion for both experiments, this then primarily becomes an issue of comparing T_{90} values derived in different bandpasses, whereas we know GRB spectral evolution tends to make a given event appear longer when measured in a lower energy bandpass (e.g. Fenimore et al. 1995). Fortunately, the *Swift* (15–350 keV) and BATSE (50–300 keV) bandpasses are similar, and we can directly measure any biases in *Swift* T_{90} values calculated in the 15–350 keV band as opposed to the 50–300 keV band. Considering 411 *Swift* GRBs, we find that the median

⁵ <ftp://legacy.gsfc.nasa.gov/swift/data>

decrease in T_{90} when considering the 50–300 keV band instead of the 15–350 keV band is only 3.8 per cent. The decrease is <30 per cent for 90 per cent of the sample, which is typically (>75 per cent of the time) contained within our 1σ error bar on T_{90} . Therefore, we expect systematic variations in T_{90} with energy band to not affect our classification.

Using the Markov Chain derived for the model division as a function of T_{90} and E_{peak} , we can directly determine the probabilistic class association for *Swift* GRBs taking into account errors in T_{90} and E_{peak} . Using a Markov Chain for this purpose effectively treats the error bars on all quantities and allows us to marginalize over the parameters describing the two-class model. The marginalization is important, because there is strong overlap in the observed BATSE distributions which translates to uncertainty in the Gaussian model parameters defining our BATSE classification. To classify the *Swift* GRBs, we sample 10^3 values for T_{90} and E_{peak} from the distributions in Butler et al. (2007). Each of these samples is used to evaluate one of the $G_1/(G_1 + G_2)$ draws above. The class probability, which is the Bayesian evidence in favour of the membership in the SHB class as compared to the LSB class, is calculated as the median of the $G_1/(G_1 + G_2)$ samples.

The ratio of Gaussians $G_1/(G_1 + G_2)$, evaluated at a particular value for T_{90} and E_{peak} , defines the probability that a given burst will belong to the SHB class under our assumptions. In the bottom panel of Fig. 1, the solid black curve shows the projection on to the abscissa of the solid distribution in the top panel. This curve is the classification marginalized over E_{peak} . Note that because we have assumed a sensitivity correction as a function of T_{90} and E_{peak} at each value of T_{90} and E_{peak} , the correction drops out of the ratio $G_1/(G_1 + G_2)$, and we can apply the BATSE $G_1/(G_1 + G_2)$ model to *Swift* without needing to account for relative sensitivity. Dashed curves are also shown to display the E_{peak} dependence of the curve at two E_{peak} values ($E_{\text{peak}} = 1$ MeV and $E_{\text{peak}} = 20$ keV, respectively).

In black circles in Fig. 1 (bottom panel), we display the probability for each *Swift* burst plotted in the top panel. We also plot as red circles the host-frame $T_{90z} = T_{90}/(1 + z)$ values for 138 GRBs with measured spectroscopic redshifts. Considering the range of observed E_{peak} values, we find that a GRB is short/hard at >90 per cent confidence if $T_{90} < 2.2$ s, or $T_{90z} < 0.8$ s. These limits can be used in future studies to select *Swift* GRBs belonging with high confidence to the short/hard class. Note that our spectroscopic redshift of $z = 2.609$ for GRB 090426 enables us to derive a rest-frame duration T_{90z} of 0.33 ± 0.08 s.

We find the probability that GRB 090426, highlighted and circled in yellow in Fig. 1, belongs to the short/hard class is 92.8 per cent. Even so, we must stress that such a high confidence indication could occur by chance given a sufficient number of detected SHBs. For ~ 400 *Swift* LSBs detected to date, the chance probability of detecting one or more long/soft GRBs with durations short enough and/or hardness high enough to appear short/hard with such high confidence in our scheme is >90 per cent. This marks a fundamental shortcoming in the classification by high-energy properties alone, where the parameter distributions suffer broad overlap, motivating further investigation into the afterglow and host properties. It is possible that additional high-energy indicators (e.g. a ‘lag’ consistent with zero; Ukwatta et al. 2009) may be useful for classification, but we do not investigate these here.

3 ENERGETICS AND AFTERGLOW

As mentioned above, from our Bayesian model of the burst parameters, we calculate an isotropic energy release of 4.2×10^{51} erg. Until

very recently, this value of E_{iso} would be considered exceptionally large for a SHB. Indeed, a low E_{iso} is naturally expected from most SHB models (Panaitescu, Kumar & Narayan 2001), which are typically assumed to collimate their ejecta less efficiently than the collapsar model (Berger 2007; Nakar 2007). However, the recent GRB 090510 (spatially associated with an emission-line galaxy) had a very large $E_{\text{iso}} = 3.8 \times 10^{52}$ erg (Rau 2009), suggesting that short-duration bursts are indeed capable of arising from very energetic (and/or tightly collimated) explosions as well, and are probably visible substantially beyond $z = 1$, even if they are not expected to be common.

Combining the (limited) set of observations of the afterglow of GRB 090426 from published circulars,⁶ we find the optical light curve is well described by a single power-law decay with index $\alpha_O \approx 0.8$ from $t \lesssim 100$ s until $t \gtrsim 4 \times 10^4$ s. This is similar to the inferred X-ray decay index, $\alpha_X \approx 0.9$, from the online compilation of NRB.⁷ Combined with the derived optical to X-ray spectral index for this interval, $\beta_{\text{OX}} \approx 0.9$, and assuming standard synchrotron afterglow theory (e.g. Sari, Piran & Narayan 1998), these results suggest an afterglow with a shallow electron index ($p \approx 1.8$) and a cooling frequency ν_c below the optical bandpass. If this is indeed the case, we can use the limit on the cooling frequency to constrain the parsec-scale circumburst density. Assuming a constant density medium, the cooling frequency falling below the optical requires (e.g. Granot & Sari 2002)

$$n \gtrsim 0.05 \epsilon_B^{-3/2} E_{\text{KE},52}^{-1/2}, \quad (1)$$

where n is the circumburst density (cm^{-3}), ϵ_B is the fraction of the shock energy partitioned to the magnetic field and $E_{\text{KE},52}$ is the kinetic energy of the outgoing blastwave (10^{52} erg). Given a maximal ϵ_B of $1/3$ at equipartition, and with $E_{\text{KE}} \lesssim 10 E_\gamma \approx 10^{53}$ erg, we derive a lower limit of $n \gtrsim 0.1 \text{ cm}^{-3}$. A similar result can be derived for the case of a wind-like circumburst medium (e.g. Chevalier & Li 1999): $A_* \gtrsim 0.01$ (where $\rho = 5 \times 10^{11} A_* \text{ g cm}^{-3}$, chosen to correspond to a mass loss rate of $\dot{M} = 10^{-5} M_\odot \text{ yr}^{-1}$ and a wind speed of $v_w = 1000 \text{ km s}^{-1}$). While we caution that this result is based on a relatively sparsely sampled optical light curve, it is clear that presence of a relatively bright and slowly fading optical and X-ray afterglow distinguish GRB 090426 from the extremely low-density circumburst environments inferred for the short GRB 080503 ($n \lesssim 5 \times 10^{-6} \text{ cm}^{-3}$; Perley et al. 2009) or the long GRB 050911 (Page et al. 2006).

4 OPTICAL AFTERGLOW SPECTROPHOTOMETRY

4.1 Observations and reductions

We obtained an optical spectrum of the afterglow of GRB 090426 using the Keck Low-Resolution Imaging Spectrometer (LRIS; Oke et al. 1995) at 13:55 on 2009 April 26, ~ 1.1 h after the BAT trigger. The observations were conducted in photometric conditions. We obtained two 300-s exposures on the LRIS blue side using the long 1 arcsec slit mask, the 680 dichroic and the 300/5000 grism. We observed internal flat-field lamps as well as spectra of Hg, Ne, Ar, Cd and Zn comparison lamps to be used for wavelength calibration. We also obtained a 60-s spectrum of the spectrophotometric standard HZ 43. The observations of the GRB 090426 afterglow were

⁶ See http://gcn.gsfc.nasa.gov/gcn3_archive.html

⁷ <http://astro.berkeley.edu/~nat/swift/>; see Butler et al. (2007) for details.

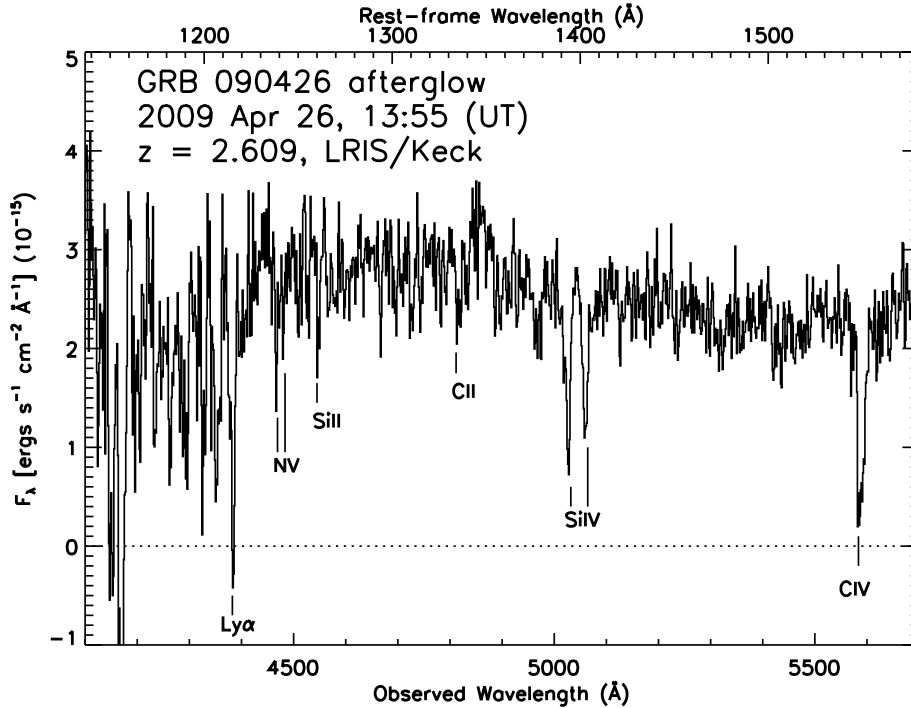


Figure 2. Keck spectrum of the GRB 090426 afterglow. The spectrum was observed with LRIS on Keck I at 13:55 on 2009 April 26, ~ 1.1 h after the BAT trigger. The observations were conducted in photometric conditions. The data were reduced using `IRAF`, and have been corrected for a heliocentric velocity of -16.88 km s^{-1} . We plot both the observed wavelength (lower abscissa) and the rest-frame wavelength at our redshift of 2.609 (upper abscissa). We note detections of the $\text{Ly}\alpha$, N v , Si II , C II , Si IV and C IV features at this redshift.

conducted at a high airmass of 3.05; HZ 43 was observed at an airmass of 3.60.

The data were reduced using `IRAF`.⁸ We used the `LRISBIAS IRAF` task distributed by the W. M. Keck Observatory to subtract overscan from the LRIS images, and apply a wavelength correction based on our internal lamp observations. The spectrum was extracted using an optimal extraction algorithm, with deviant pixels identified and rejected based upon the assumption of a smoothly varying profile. We flux calibrated the data using observations of HZ 43 to derive a sensitivity curve which was then applied to the GRB 090426 afterglow observation. Finally, we corrected for a heliocentric velocity of -16.88 km s^{-1} and corrected the spectrum to rest-frame wavelengths. Our spectrum is shown in Fig. 2.

4.2 Analysis and interpretation

In our analysis of the afterglow spectrum, we initially observed a set of absorption features at 4387, 5030, 5061 and 5592 Å. We identify these features as $\text{Ly}\alpha$, $\text{Si IV } \lambda 1394$, $\text{Si IV } \lambda 1403$ and the blended $\text{C IV } \lambda\lambda 1548, 1551$ doublet at a common redshift of $z = 2.609$. At this redshift we are also able to identify the $\text{N v } \lambda\lambda 1239, 1243$ doublet, $\text{Si II } \lambda 1260$ and $\text{C II } \lambda 1334$ absorption features. We determine the rest-frame equivalent widths (EWs) for these lines by fitting each line with a Gaussian using `SPLIT` in `IRAF`.

We find that the ionized absorption lines in our spectrum are saturated, which limits us to determining conservative lower limits for the column densities of these lines (Prochaska 2006) based on the relation between EW and column density for saturated lines

Table 1. Species detected in the Keck/LRIS GRB 090426 afterglow spectrum.

Species (λ_0)	EW ₀ (Å)	N_X (cm^{-2})
$\text{Ly}\alpha$ (1215.67 Å)	2.8 ± 0.1	$< 3.2 \times 10^{19}$
N v (1238.82 Å)	0.7 ± 0.1	$> 2.8 \times 10^{14}$
N v (1242.80 Å)	0.3 ± 0.1	$> 1.8 \times 10^{14}$
Si II (1260.42 Å)	0.6 ± 0.1	$> 3.8 \times 10^{13}$
C II (1334.53 Å)	0.3 ± 0.1	$> 1.0 \times 10^{14}$
Si IV (1393.75 Å)	2.2 ± 0.1	$> 3.2 \times 10^{14}$
Si IV (1402.77 Å)	1.7 ± 0.1	$> 3.7 \times 10^{14}$
C IV (1548.20 Å/1550.78 Å)	3.6 ± 0.1	$> 9.1 \times 10^{14}$

Note. EW₀ and λ_0 are given in rest-frame quantities.

(Cowie & Songaila 1986). We generally find lower limits for all the saturated columns on the order of 10^{14} cm^{-2} . However, we are able to calculate an upper limit for $N_{\text{H I}}$ based on the absence of strong damping wings in the $\text{Ly}\alpha$ absorption feature. From fitting the line with a Voigt profile, we find an upper limit of $N_{\text{H I}} < 3.2 \times 10^{19} \text{ cm}^{-2}$. Our values for EW and the various column densities are given in Table 1.

The value of the neutral hydrogen column is very low in comparison to other GRBs: based on the cumulative distribution of $N_{\text{H I}}$ in 28 long-duration GRBs at $z \geq 2$ (Chen, Prochaska & Gnedin 2007), we find that the afterglow of GRB 090426 has a lower $N_{\text{H I}}$ than ~ 90 per cent of GRB afterglow spectra. Our GRB 090426 afterglow spectrum also appears to have weaker low-ionization absorption (Si II , C II) than ~ 95 per cent of previous afterglow spectra. This sets GRB 090426 apart as atypical when compared to the host environments of other GRBs, which generally have much stronger absorption features (Prochaska et al. 2008). Nevertheless, even among ‘typical’ long-duration GRBs, such very low columns are not

⁸ `IRAF` is distributed by NOAO, which is operated by AURA, Inc., under cooperative agreement with the NSF.

completely without precedent, and a few long-duration GRB afterglow spectra are found to have similarly low $N_{\text{H I}}$ to GRB 090426. Typically, GRB afterglows with Ly α lines have column densities of $N_{\text{H I}} \approx 10^{21} \text{ cm}^{-2}$; one notable exception is GRB 021004, which has $N_{\text{H I}} \approx 1 \times 10^{19} \text{ cm}^{-2}$. It is suggested that the low measured $N_{\text{H I}}$ in that afterglow spectrum is due to ionization of the H I by the radiation field of the massive-star progenitor (Fynbo et al. 2005). Another unusual afterglow is associated with the long/soft GRB 060607; with $N_{\text{H I}} = 6.3 \times 10^{16} \text{ cm}^{-2}$, it has the lowest H I column density of any GRB afterglow. The GRB 060607 spectrum lacks any detection of the N v lines, though it does show C IV and Si IV absorption at the redshift of the GRB (Prochaska et al. 2008). However, no host galaxy has been detected for GRB 060607 thus far, down to an H -band limiting magnitude of $AB(H) = 26.5$ (Chen et al. 2009). By contrast, we do in fact detect the N v doublet in the afterglow spectrum of GRB 090426. N v is thought to originate in the immediate circumburst environment of the GRB, and this absorption feature is quite typical of most other observed GRB afterglows (Prochaska et al. 2008).

Similarly, examples of systems with extremely weak low-ionization lines, while quite rare, are not unprecedented among ordinary long bursts: GRB 070125 and GRB 071003 were both found to have extremely weak host Mg II absorption systems (Cenko et al. 2008; Perley et al. 2008), indicative of a low-density galactic environment, possibly in a tidal tail or halo.

5 THE HOST GALAXY OF GRB 090426

5.1 Imaging

On 2009 May 21 we imaged the field using GMOS-S on Gemini-South and the i -band filter for 20 exposures of 180 s each, for 1 h of total integration time. Images were processed using archival twilight flat-fields and fringe corrected within the GEMINI package in IRAF.

The following night (2009 May 22) we acquired additional imaging in the V band using the FOCAS instrument on Subaru. A total of nine images of 300 s each were acquired for a total integration time of 45 min. Images were processed using standard techniques in IRAF. Both optical images show a bright, extended object with complicated morphology (a bright, elongated object with fainter lobes of emission to the north-east and south) near the afterglow location (Fig. 3).

Finally, on 2009 May 31 we imaged the field using NIRC on the Keck I telescope. A total of 31 exposures of 1 min (10 co-adds \times 6 s) were acquired in the K band, plus nine in the H band (also 10 \times 6 s) and nine in the J band (3 \times 20 s). Images were processed and stacked using a modified *Python/pyraf* script originally written by D. Kaplan. No object consistent with the optical band is detected in any filter. Based on a calibration to Two Micron All Sky Survey (2MASS) standards observed in frames taken later in the night, we place 3σ limiting magnitudes on the host-galaxy flux of $J > 23.0$, $H > 22.1$ and $K > 22.0$ mag (Vega).

To calculate the offset of the afterglow relative to the putative host galaxy, we aligned both the LRIS acquisition image (taken the night of the burst) and the Subaru V -band observation to reference stars in the Sloan Digital Sky Survey, giving a position of $\alpha = 12^{\text{h}}36^{\text{m}}18^{\text{s}}.052$, $\delta = +32^{\circ}59'09''.14$ (J2000). This position places the afterglow within 0.1 arcsec (800 pc in projection) of the centre of the north-eastern lobe of the system that we subsequently identify as the host galaxy complex.

Aperture photometry of the brightest (central) region of the host as well as the knot at the afterglow location was performed with IRAF using a 1-arcsec radius. The resulting photometry, corrected for the modest Galactic extinction [$E(B - V) = 0.017$ mag; Schlegel, Finkbeiner & Davis 1998], is presented in Table 2. In addition to the spatial coincidence, the identical colours strongly suggest that the two objects are physically related. Interpolating to the flux at 1700 Å (see Reddy et al. 2008), the photometric magnitude of the

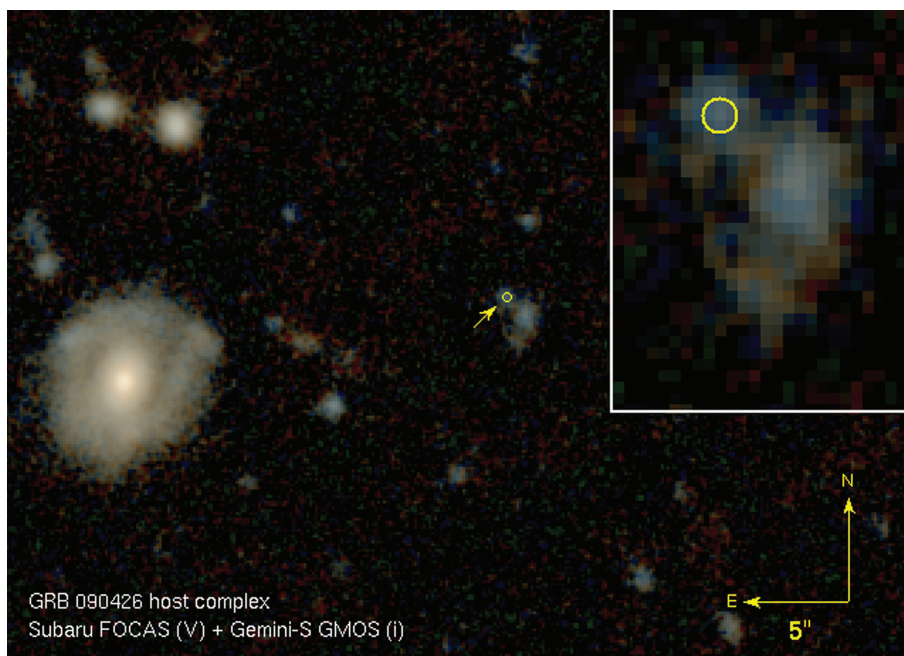


Figure 3. False-colour optical image of the host-galaxy field from combined i -band data from GMOS-S on Gemini South and V -band data from FOCAS on Subaru. A magnified region of the host complex is inset at top right. The afterglow position identified by our LRIS acquisition imaging is shown in both images as a yellow circle of radius 0.2 arcsec (2σ) and is consistent with the north-east component of the complex. The large galaxy 18 arcsec to the east of the host complex is that noted by D’Avanzo et al. (2009).

Table 2. Photometry of the GRB 090426 host-galaxy complex.

Filter	Date (2009 UT)	Telescope/instrument	Extended host (AB magnitude)	Compact knot (AB magnitude)
<i>V</i>	May 22.26	Subaru/FOCAS	24.21 ± 0.15	24.73 ± 0.15
<i>i'</i>	May 21.05	Gemini South/GMOS	24.09 ± 0.15	24.61 ± 0.18
<i>J</i>	May 31.30	Keck I/NIRC	>23.9	>23.9
<i>H</i>	May 31.30	Keck I/NIRC	>23.5	>23.5
<i>K_s</i>	May 31.35	Keck I/NIRC	>23.8	>23.8

north-east component of the host corresponds to a rest-frame UV luminosity of approximately $0.7L_*$, or $\sim 2L_*$ for the entire host complex, indicating a luminous host galaxy.

5.2 Spectroscopy

We obtained an additional late-time spectrum at the afterglow location with LRIS on 2009 June 17. Extrapolating the early-time optical light curve, the afterglow flux should have faded sufficiently such that any emission would be dominated by host-galaxy light. Our observations consisted of two 1500-s exposures. The blue side was configured with the 600/4000 grism, providing coverage of 3500–5500 Å with a scale of 0.62 arcsec pixel⁻¹, and a spectral resolution of ~ 4 Å. The red side employed the 400/8500 grating with wavelength coverage of 5500–10000 Å, a scale of 1.18 arcsec pixel⁻¹, and a spectral resolution of ~ 7 Å; however, we do not discuss the red-side spectrum here, since we are interested primarily in a detection of Ly α emission from the host galaxy. The long, 1-arcsec-wide slit was oriented with a position angle of 41:3 to capture both the compact ‘knot’ at the afterglow location and the nearby extended galaxy, while an atmospheric dispersion corrector was utilized to account for differential refraction (Filippenko 1982). We are confident that the slit was at the correct location, because we detected another object at its expected position along the spatial axis of the spectrogram.

The spectra were reduced in a manner identical to that described in Section 3.1. We find no sign of any flux, either continuum or narrow emission lines, at the location of the afterglow or host complex. At $z = 2.609$, Ly α would fall at $\lambda_{\text{obs}} = 4389$ Å. Using observations of the standard star Feige 34 (Massey et al. 1988; Oke 1990; Stone 1996) from earlier in the night, we place a limit on any emission-line flux at this location of $F < 7 \times 10^{-17}$ erg cm⁻² s⁻¹ (assuming the line was narrow enough to be unresolved in our spectra). Using the star formation rate (SFR) conversions from Brocchehurst (1971) and Kennicutt (1983), we therefore place a limit on the unobscured SFR at the location of the afterglow and host of $\text{SFR}_{\text{Ly}\alpha} < 4 M_{\odot} \text{ yr}^{-1}$. This value is significantly less than that derived from the k -corrected rest-frame UV (1500 Å) continuum emission (neglecting extinction corrections), where $\text{SFR}_{\text{UV}} = 14.4 \pm 2.0 M_{\odot} \text{ yr}^{-1}$ (Kennicutt 1998). However, we note that SFRs derived from Ly α emission can often underestimate the true SFR by over an order of magnitude due to resonant scattering, dust absorption (Mass-Hesse et al. 2003) and a strong dependency on the age of the star-forming population (e.g. Valls-Gabaud 1993). Furthermore, the night of these spectroscopic observations was not photometric (variable, thin cloud cover), and therefore our flux calibration may be in error (though likely at less than the 50 per cent level). It is also worth noting that ~ 50 per cent of obviously star-forming Lyman break galaxies show Ly α in absorption rather than emission; therefore, the non-detection of Ly α in this case is not conclusive.

5.3 Models and interpretation

We generated synthetic photometry in our measured filters at $z = 2.609$ using the irregular, Sc/d, Sb/c and elliptical-galaxy templates in hyper-Z (Bolzonella, Miralles & Pelló 2000; templates originally from Coleman, Wu & Weedman 1980). The templates were screened by varying amounts of host-galaxy dust, both with and without the 2175 Å bump [assuming an Large Magellanic Cloud (LMC) and Small Magellanic Cloud (SMC) extinction law, respectively] to compare with the observed colours. The elliptical and Sb/c models were immediately ruled out as incompatible with the blue $i - K$ colour implied by the NIRC non-detections, as were large amounts of dust extinction in any case. The highly starburst-dominated irregular template (plus a small amount of extinction, $A_V \approx 0.4$ mag) is favoured over the slightly more evolved Sc/d template, though given the limited photometry available and the simplified nature of the modelling this conclusion is less robust. From this examination, it is clear that the broad-band photometry indicates a stellar population dominated by young stars.

5.4 Associating the galaxy complex with GRB 090426

In the optical afterglow spectrum we find no detections of any intervening absorption systems at a redshift of $z < 2.609$. Similarly, in our spectroscopic observations of the putative host complex at the position of the afterglow we see no spectral features that would be consistent with contributions from a foreground system.

In the absence of an emission-line redshift of the complex, it is reasonable to ask what the possibility is that this host association is the result of a chance alignment between GRB 090426 and a foreground system at $z < 2.609$ (at z_{complex} much larger than z_{abs} the system would be too bright intrinsically). Examining only the north-eastern lobe of the host complex and following the prescription in Bloom et al. (2002), we estimate a probability of chance alignment between afterglow and the central region of its host galaxy (using an effective radius of 0.25 arcsec) to be 0.1 per cent. More conservatively, if we instead consider the entire host complex (approximately 1.8-arcsec radius), the probability of chance alignment is still low at 4 per cent. Based on the low likelihood of a chance alignment and a lack of spectroscopic evidence supporting the presence of a foreground system, we conclude that this is indeed very likely the host galaxy (complex) of GRB 090426.

6 CONCLUSIONS

The small astrometric offset from what appears to be a blue host galaxy initially seems to be difficult to square with the inference of a very low column density implied by the absorption spectrum. However, it is noteworthy that the upper limit probes only the neutral gas; the implied UV luminosity from the bright host system suggests a large ionizing radiation field in and around the galactic discs

which may have ionized a significant fraction of the neutral gas along the line of sight to the GRB. Furthermore, both the detection of N v and the significant circumburst density implied by the bright afterglow indicate that the immediate environment of GRB 090426 is not dramatically different from those of long-duration GRBs in general.

Some degenerate merger scenarios (the merging of two neutrons stars, for example) involve a significant (> 1 Gyr) delay between initial formation of the system and the merger. This in turn suggests that the positional and temporal coincidence of the afterglow with what could be a starburst induced by tidal interaction with the nearby object would be relatively unlikely. In these scenarios, the progenitor system is also subject to a systemic velocity ‘kick’ during binary evolution that results in significant linear motion of the system away from its birthsite (Bloom, Sigurdsson & Pols 1999; Fryer, Woosley & Hartmann 1999; although see also Belczynski, Kalogera & Bulik 2002). For instance, a binary with a 100 km s^{-1} kick perpendicular to our line of sight that takes 1 Gyr to merge will travel 100 kpc from its birthsite; in our adopted cosmology⁹ at $z = 2.609$ this amounts to an angular distance of 12.8 arcsec, compared to the observed < 0.2 arcsec offset.

This does not preclude the possibility that this event could have arisen from a merger-product progenitor; if such progenitors can merge over a range of time-scales (including relatively short ones), the association of SHBs with active starbursts would be no surprise. If GRB 090426 is interpreted as arising from a merger, this event may suggest that SHBs may very well be akin to Type Ia supernovae (which appear to be generated by both long and short production channels; Sullivan et al. 2006). Indeed, many SHBs to date have shown little to no appreciable offset from their (sometimes blue) host galaxies (Troja et al. 2008). This event also serves as a spectroscopic example of the high-redshift short-duration GRB population inferred from spatial associations in Berger (2007). While the most direct evidence for a degenerate merger remains the detection of a gravity wave signature (see for example Bloom et al. 2009), then GRB 090426, at a large redshift with large E_{iso} , would suggest (cf. Berger 2007; Berger 2009) unfortunately that a significant number of SHBs detected by BATSE and *Swift* occur well outside of the Advanced LIGO volume.

However, the most conservative conclusion from the available observations of the afterglow and host galaxy is that GRB 090426 is more closely linked with a massive star progenitor. The implications of this association are no less profound: they indicate that the mechanism that generates gamma-rays in the death of a massive star is capable of operating on time-scales as short as 0.3 s, imposing strong demands of the central engine; in the most basic collapsar model for GRBs, the duration time-scale is generally assumed to be at least an order of magnitude longer (see Woosley & Bloom 2006). While events like GRB 090426 are probably rare (due to relative volumetric effects), these inferences also cast significant doubt on the classification of a large population of what would otherwise have been considered classical short-duration bursts: if this burst had occurred at a similar redshift to prototypical SHBs 050509B or 050724 (at $z = 0.2\text{--}0.3$) it would have fallen unambiguously within the SHB duration distribution. This also illustrates the insufficiency of T_{90} alone as a classification criterion, given the 92.8 per cent likelihood that GRB 090426 is a member of the short/hard phenomenological class. At minimum, we feel that at low redshift, the search for accompanying supernova emission – an unambigu-

ous sign of a genuine massive-star origin – remains vital to properly distinguishing among different progenitor scenarios.

ACKNOWLEDGMENTS

Some of the data presented herein were obtained at the W. M. Keck Observatory, which is operated as a scientific partnership among the California Institute of Technology, the University of California and NASA; the observatory was made possible by the generous financial support of the W. M. Keck Foundation. We wish to thank the support staff of the W. M. Keck Observatory, Subaru telescope and Gemini Observatory for their hospitality and assistance. We also thank to Jeff Silverman for his assistance during our observations. This paper made use of data from the Gamma-Ray Burst Coordinates Network (GCN) circulars. EML’s participation was made possible in part by a Ford Foundation Predoctoral Fellowship. JSB’s group is supported in part by Las Cumbres Observatory Global Telescope Network, and NASA/*Swift* Guest Investigator grant NNG05GF55G. NRB is partially supported by US Department of Energy (DOE) SciDAC grant DE-FC02-06ER41453 and through the GLAST Fellowship Program (NASA Cooperative Agreement: NNG06DO90A). JXP is partially supported by NASA/*Swift* grant NNX07AE94G and an NSF CAREER grant (AST-0548180). AVF and his group are grateful for funding from US NSF grant AST-0607485, NASA/*Swift* grant NNG06GI86G, DOE/SciDAC grant DE-FC02-06ER41453, the TABASGO Foundation, Gary and Cynthia Bengier and the Richard and Rhoda Goldman Fund. MM is supported by a research fellowship from the Miller Institute for Basic Research in Science. SL was partly supported by the Chilean *Centro de Astrofísica* FONDAF No. 15010003 and by FONDECYT grant No. 1060823.

REFERENCES

- Abbott B. et al., 2008, *ApJ*, 681, 1419
 Band D. L., 2006, *ApJ*, 644, 378
 Band D. et al., 1993, *ApJ*, 413, 281
 Barthelmy S. D. et al., 2005, *Space Sci. Rev.*, 120, 143
 Belczynski K., Kalogera V., Bulik T., 2002, *ApJ*, 572, 407
 Berger E., 2007, *ApJ*, 670, 1254
 Berger E., 2009, *ApJ*, 690, 231
 Berger E. et al., 2005, *Nat*, 438, 988
 Berger E. et al., 2007, *ApJ*, 664, 1000
 Bloom J. S., Prochaska J. X., 2006, in Holt S. S., Gehrels N., Nousek J. A., eds, *AIP Conf. Ser. Vol. 836, Gamma-Ray Bursts in the Swift Era*. Am. Inst. Phys., New York, p. 473
 Bloom J. S., Sigurdsson S., Pols O. R., 1999, *MNRAS*, 305, 763
 Bloom J. S., Kulkarni S. R., Djorgovski S. G., 2002, *AJ*, 123, 1111
 Bloom J. S. et al., 2006, *ApJ*, 638, 354
 Bloom J. S. et al., 2007, *ApJ*, 654, 878
 Bloom J. S., Butler N. R., Perley D. A., 2008, in Galassi M., Palmer D., Fenimore E., eds, *AIP Conf. Ser. Vol. 1000, Gamma-Ray Bursts, Classified Physically*. Am. Inst. Phys., New York, p. 11
 Bloom J. S. et al., 2009, preprint (arXiv:0902.1527)
 Bolzonella M., Miralles J.-M., Pelló R., 2000, *A&A*, 363, 476
 Brocklehurst M., 1971, *MNRAS*, 153, 471
 Burrows D. N. et al., 2005, *Space Sci. Rev.*, 120, 165
 Butler N. R., Kocevski D., Bloom J. S., Curtis J. L., 2007, *ApJ*, 671, 656
 Castro-Tirado A. J. et al., 2008, *Nat*, 455, 506
 Cenko S. B. et al., 2008, *ApJ*, 677, 441
 Chapman R., Priddey R. S., Tanvir N. R., 2009, *MNRAS*, 395, 1515
 Chen H.-W., Prochaska J. X., Gnedin N. Y., 2007, *ApJ*, 667, L125
 Chen H.-W. et al., 2009, *ApJ*, 691, 152
 Chevalier R. A., Li Z.-Y., 1999, *ApJ*, 520, L29
 Coleman G. D., Wu C.-C., Weedman D. W., 1980, *ApJS*, 43, 393
 Cowie L. L., Songaila A., 1986, *ARA&A*, 24, 499

⁹ $H_0 = 72 \text{ km s}^{-1} \text{ Mpc}^{-1}$, $\Omega_m = 0.3$, $\Omega_\Lambda = 0.7$.

- Cummings J. R. et al., 2009, GRB Coordinates Network, 9254, 1
- Curtis J. L., Butler N., Bloom J., Kocevski D., 2006, BAAS, 38, 1290
- D’Avanzo P., Palazzi E., Thoene C. C., Maiorano E., Chincarini G., Antonelli L. A., Piranomonte S., 2009, GRB Coordinates Network, 9256, 1
- de Ugarte Postigo A. et al., 2006, ApJ, 648, L83
- Fenimore E. E., in’t Zand J. J. M., Norris J. P., Bonnell J. T., Nemiroff R. J., 1995, ApJ, 448, L101
- Filippenko A. V., 1982, PASP, 94, 715
- Fox D. B. et al., 2005, Nat, 437, 845
- Fruchter A. S. et al., 2006, Nat, 441, 463
- Fryer C. L., Woosley S. E., Hartmann D. H., 1999, ApJ, 526, 152
- Fynbo J. P. U. et al., 2005, ApJ, 633, 317
- Fynbo J. P. U. et al., 2006, Nat, 444, 1047
- Gehrels N. et al., 2004, ApJ, 611, 1005
- Gehrels N. et al., 2006, Nat, 444, 1044
- Granot J., Sari R., 2002, ApJ, 568, 820
- Gregory P. C., 2005, Bayesian Logical Data Analysis for the Physical Sciences: A Comparative Approach with ‘Mathematica’ Support. Cambridge Univ. Press, Cambridge
- Greiner J. et al., 2009, ApJ, 693, 1610
- Hjorth J. et al., 2003, Nat, 423, 847
- Hjorth J. et al., 2005, ApJ, 630, L117
- Hurley K., 2008, Chinese J. Astron. Astrophys. Suppl., 8, 202
- Jakobsson P., Fynbo J. P. U., 2007, preprint (arXiv:0704.1421)
- Kaneko Y., Preece R. D., Briggs M. S., Paciesas W. S., Meegan C. A., Band D. L., 2006, ApJS, 166, 298
- Kasliwal M. M. et al., 2008, ApJ, 678, 1127
- Kennicutt R. C., Jr., 1983, ApJ, 272, 54
- Kennicutt R. C., Jr., 1998, ARA&A, 36, 189
- Kouveliotou C., Meegan C. A., Fishman G. J., Bhat N. P., Briggs M. S., Koshut T. M., Paciesas W. S., Pendleton G. N., 1993, ApJ, 413, L101
- Lee W. H., Ramirez-Ruiz E., 2007, New J. Phys., 9, 17
- Levan A. J. et al., 2006, ApJ, 648, L9
- Levesque E. M., Kewley L. J., 2007, ApJ, 667, L121
- Levesque E., Chornock R., Kewley L., Bloom J. S., Prochaska J. X., Perley D. A., Cenko S. B., Modjaz M., 2009, GRB Coordinates Network, 9264, 1
- Lu Y., Huang Y. F., Zhang S. N., 2008, in Huang Y.-F., Dai Z.-G., Zhang B., eds, AIP Conf. Ser. Vol. 1065, The Origin of the Gamma-Ray Burst of GRB 060614. Am. Inst. Phys., New York, p. 285
- Mas-Hesse J. M., Kunth D., Tenorio-Tagle G., Leitherer C., Terlevich R. J., Terlevich E., 2003, ApJ, 598, 858
- Massey P., Strobel K., Barnes J. V., Anderson E., 1988, ApJ, 328, 315
- Modjaz M. et al., 2008, AJ, 135, 1136
- Nakar E., 2007, Phys. Rep., 442, 166
- Oke J. B., 1990, AJ, 99, 1621
- Oke J. B. et al., 1995, PASP, 107, 375
- Page K. L. et al., 2006, ApJ, 637, L13
- Panaitescu A., Kumar P., Narayan R., 2001, ApJ, 561, L171
- Perley D. A. et al., 2008, ApJ, 688, 470
- Perley D. A. et al., 2009, ApJ, 696, 1871
- Preece R. D., Briggs M. S., Mallozzi R. S., Pendleton G. N., Paciesas W. S., Band D. L., 2000, ApJS, 126, 19
- Prochaska J. X., 2006, ApJ, 650, 272
- Prochaska J. X. et al., 2006, ApJ, 642, 989
- Prochaska J. X., Dessauges-Zavadsky M., Ramirez-Ruiz E., Chen H.-W., 2008, ApJ, 685, 344
- Rau A., 2009, GRB Coordinates Network, 9353, 1
- Reddy N. A., Steidel C. C., Pettini M., Adelberger K. L., Shapley A. E., Erb D. K., Dickinson M., 2008, ApJS, 175, 48
- Roming P. W. A. et al., 2005, Space Sci. Rev., 120, 95
- Salvaterra R. et al., 2009, preprint (arXiv:0906.1578)
- Sari R., Piran T., Narayan R., 1998, ApJ, 497, L17
- Savaglio S., Glazebrook K., LeBorgne D., 2009, ApJ, 691, 182
- Schlegel D. J., Finkbeiner D. P., Davis M., 1998, ApJ, 500, 525
- Stanek K. Z. et al., 2003, ApJ, 591, L17
- Stanek K. Z. et al., 2006, Acta Astron., 56, 333
- Stone R. P. S., 1996, ApJS, 107, 423
- Sullivan M. et al., 2006, ApJ, 648, 868
- Tanvir N. R. et al., 2009, preprint (arXiv:0906.1577)
- Thöne C. C. et al., 2008, ApJ, 676, 1151
- Thöne C. C. et al., 2009, GRB Coordinates Network, 9269, 1
- Troja E., King A. R., O’Brien P. T., Lyons N., Cusumano G., 2008, MNRAS, 385, L10
- Ukwatta T. N., Gehrels N., Krimm H. A., Sakamoto T., Barthelmy S. D., Stamatikos M., 2009, GRB Coordinates Network, 9272, 1
- Valls-Gabaud D., 1993, ApJ, 419, 7
- van Dyk D. A., Connors A., Kashyap V. L., Siemiginowska A., 2001, ApJ, 548, 224
- Wainwright C., Berger E., Penprase B. E., 2007, ApJ, 657, 367
- Woosley S., Bloom J. S., 2006, ARA&A, 44, 507
- Xin L. P., Zheng W. K., Qiu Y. L., Wei J. Y., Wang J., Deng J. S., Urata Y., Hu J. Y., 2009, GRB Coordinates Network, 9255, 1
- Xu D. et al., 2009, ApJ, 696, 971
- Zhang Z.-B., Choi C.-S., 2008, A&A, 484, 293
- Zhang B., Mészáros P., 2004, Int. J. Modern Phys. A, 19, 2385
- Zhang B., Zhang B.-B., Liang E.-W., Gehrels N., Burrows D. N., Mészáros P., 2007, ApJ, 655, L25
- Zhang B. et al., 2009, ApJ, 703, 1696

APPENDIX A: DETERMINATION OF THE BATSE HARDNESS DURATION DISTRIBUTIONS FOR SWIFT

To estimate E_{peak} for the largest possible number of BATSE GRBs (1728 from the current BATSE catalogue),¹⁰ we determine a relationship between the BATSE catalogue hardness ratio (HR) and the measured E_{peak} from Kaneko et al. (2006) for 325 GRBs in common. We find $E_{\text{peak}} \approx 80(\text{HR}_{3412})^{0.69}$ keV, with a scatter of 0.3 dex. Here, HR_{3412} is the hardness ratio of fluences in BATSE bands 3 + 4 over 1 + 2.

We fit a double elliptical Gaussian model to the observed distributions in T_{90} and E_{peak} from BATSE. Assuming a Gaussian shape entails making the fewest assumptions on the true underlying distributions, because a Gaussian is the maximum-entropy distribution in the case of known mean and variance (e.g. Gregory 2005). We employ a Markov Chain Monte Carlo algorithm based on the data augmentation algorithm in van Dyk et al. (2001) to propagate errors and marginalize over the thirteen Gaussian parameters defining the best-fitting, two-class model shown in blue in Fig. 1 (top panel). We begin by stochastically dividing the BATSE observations between classes, given an initial guess for the Gaussian parameters and also samples for the T_{90} and E_{peak} values from their respective best-fitting distributions (assumed Gaussian). With this division in place, we find the best-fitting Gaussian parameters again and draw samples for each from the posterior distribution using the Gibbs sampling technique (e.g. van Dyk et al. 2001). The process is iterated, allowing us to determine 10^3 samples for each parameter after dropping 100 samples (‘burn in’) to allow the chain to converge.

We scale the best-fitting double-class model by the relative sensitivity curve to obtain the contours in black in Fig. 1, which are those expected for *Swift*. To do the scaling, we must assume a relation for the number of bursts gained (lost) as the sensitivity is decreased (increased). We assume that the number scales as the relative sensitivity to some power η . This η is the slope of the cumulative number density versus flux relation (i.e. the $\log N$ – $\log S$ relation, as in Preece et al. 2000). We take $\eta = -0.75$. The sensitivity curves as a function of E_{peak} and T_{90} duration are taken from figs 3 and 4 of Band (2006). The curves we use assume an exponential burst light

¹⁰ <http://www.batse.msfc.nasa.gov/batse/grb/catalog/current>

curve and a Band et al. (1993) model with $\alpha = -1$ and $\beta = -2$. Our resulting black curves do appear to better match the *Swift* T_{90} and E_{peak} distributions (Fig. 1, top panel).

To quantitatively judge the validity of the corrected model, we determine the rate increase/decrease factor for each GRB as a function of E_{peak} and T_{90} in the *Swift* sample and generate from these a corrected T_{90} histogram. The Kolmogorov–Smirnov (KS) test probability that the uncorrected distributions from *Swift* and BATSE are the same is 10^{-6} ; however, with application of the relative sensitivity function to adjust the rate for each event, the KS-test probability is

only 2.7 per cent. Hence, the distributions become only marginally inconsistent with no ad hoc changes. More precise tweaking, which would utilize the exact spectral/temporal properties and a detailed simulation of the *Swift* trigger algorithm, would likely improve the consistency, although this analysis would be very challenging to conduct and is beyond the scope of this work. For further discussion see Butler et al. (in preparation).

This paper has been typeset from a $\text{\TeX}/\text{\LaTeX}$ file prepared by the author.